

1

Nighttime atmospheric chemistry of iodine

2 Alfonso Saiz-Lopez¹, John M.C. Plane², Carlos A. Cuevas¹, Anoop S. Mahajan³, Jean-François
3 Lamarque⁴ and Douglas E. Kinnison⁴

4 ¹Department of Atmospheric Chemistry and Climate, Institute of Physical Chemistry
5 Rocasolano, CSIC, Madrid, Spain

6
7 ²School of Chemistry, University of Leeds, Leeds, UK

8
9 ³Indian Institute of Tropical Meteorology, Pune, India

10
11 ⁴Atmospheric Chemistry Observations and Modelling, NCAR, Colorado, USA

12 Correspondence to: A. Saiz-Lopez (a.saiz@csic.es)

1 **Abstract**

2 Little attention has so far been paid to the nighttime atmospheric chemistry of iodine species.
3 Current atmospheric models predict a buildup of HOI and I₂ during the night that leads to a spike
4 of IO at sunrise, which is not observed by measurements. In this work, electronic structure
5 calculations are used to survey possible reactions that HOI and I₂ could undergo at night in the
6 lower troposphere, and hence reduce their nighttime accumulation. The new reaction NO₃ + HOI
7 → IO + HNO₃ is proposed, with a rate coefficient calculated from statistical rate theory over the
8 temperature range 260 - 300 K and at a pressure of 1000 hPa to be $k(T) = 2.7 \times 10^{-12} (300 \text{ K} / T$
9 $)^{2.66} \text{ cm}^3 \text{ molecule}^{-1} \text{ s}^{-1}$. This reaction is included in two atmospheric models, along with the
10 known reaction between I₂ and NO₃, to explore a new nocturnal iodine radical activation
11 mechanism. The results show that this iodine scheme leads to a considerable reduction of
12 nighttime HOI and I₂, which results in the enhancement of more than 25% of nighttime ocean
13 emissions of HOI + I₂ and the removal of the anomalous spike of IO at sunrise. We suggest that
14 active nighttime iodine can also have a considerable, so far unrecognized, impact on the
15 reduction of the NO₃ radical levels in the marine boundary layer (MBL) and hence upon the
16 nocturnal oxidizing capacity of the marine atmosphere. The effect of this is exemplified by the
17 indirect effect on dimethyl sulfide (DMS) oxidation.

18

19

20

21

1 **1. Introduction**

2 Active nighttime iodine chemistry was first evidenced a decade ago when it was shown that
3 nocturnal I₂ emitted by macroalgae could react with NO₃ leading to the formation of IO and
4 OIO, which were measured in the coastal MBL at Mace Head, Ireland (Saiz-Lopez and Plane,
5 2004). The nitrate radical has also been recently suggested as a nocturnal loss of CH₂I₂, which
6 helps to reconcile observed and modelled concentrations of this iodocarbon over the remote
7 MBL (Carpenter et al., 2015). However, most of the work on reactive atmospheric iodine has
8 focused on the use of daytime observations and models to assess its role in the catalytic
9 destruction of ozone and the oxidizing capacity of the troposphere (e.g. Saiz-Lopez et al. (2012b)
10 and references therein). In the MBL, iodine-, along with bromine-catalysed ozone destruction
11 contributes up to 45% of the observed daytime depletion (Read et al., 2008; Mahajan et al.,
12 2010a), although this contribution shows large geographical variability (Mahajan et al., 2012;
13 Gómez Martín et al., 2013; Prados-Roman et al., 2015b; Volkamer et al., 2015). Iodine
14 compounds have also been implicated in the formation of aerosols, although the mechanisms and
15 magnitudes of these processes are not fully understood (Hoffmann et al., 2001; O'Dowd et al.,
16 2002; McFiggans et al., 2004; Gomez Martin et al., 2013; Allan et al., 2015; Roscoe et al., 2015).
17 Reactive forms of inorganic iodine may also contribute to the oxidation of elemental mercury
18 over the tropical oceans (Wang et al., 2014). In recent years, iodine sources and chemistry have
19 also been implemented in global models demonstrating the effect of iodine chemistry in the
20 oxidation capacity of the global marine troposphere (Ordóñez et al., 2012; Saiz-Lopez et al.,
21 2012a; Saiz-Lopez et al., 2014; Sherwen et al., 2016).

22 Iodine is emitted into the atmosphere from the ocean surface in both organic and inorganic
23 forms. The main organic compounds emitted are methyl iodide (CH₃I), ethyl iodide (C₂H₅I),

1 propyl iodide (1- and 2-C₃H₇I), chloriodomethane (CH₂ICl), bromiodomethane (CH₂IBr), and
2 diiodomethane (CH₂I₂) (Carpenter, 2003; Butler et al., 2007; Jones et al., 2010; Mahajan et al.,
3 2012). However, these organic compounds contribute only up to a fourth of the MBL iodine
4 loading (Jones et al., 2010; Mahajan et al., 2010a; Großmann et al., 2013; Prados-Roman et al.,
5 2015b). Inorganic emissions of HOI and I₂, which result from the deposition of O₃ at the ocean
6 surface and subsequent reaction with I⁻ ions in the surface microlayer, account for the main
7 source of iodine in the MBL (Carpenter et al., 2013). Recent laboratory experiments have shown
8 that HOI is the major compound emitted, and provided parameterizations of the fluxes of both
9 species depending on wind speed, temperature, and the concentrations of O₃ and I⁻ (Carpenter et
10 al., 2013; MacDonald et al., 2014). These parameterized fluxes of HOI and I₂ have then been
11 used in a one-dimensional model to study the diurnal evolution of the IO and I₂ mixing ratios at
12 the Cape Verde Atmospheric Observatory (CVAO) (Carpenter et al., 2013; Lawler et al., 2014).
13 The model simulations replicate well the levels and general diurnal profiles of IO and I₂,
14 although an early morning ‘dawn spike’ in IO is predicted by the models, but has not been
15 observed (Read et al., 2008; Mahajan et al., 2010a). The morning peak predicted by current
16 iodine chemistry models is due to a buildup of the emitted I₂ and HOI (which is converted into
17 IBr/ICl through heterogeneous sea-salt recycling) over the course of the night, followed by rapid
18 photolysis at sunrise.

19 Traditionally it has been thought that iodine chemistry has a negligible effect on oxidizing
20 capacity of the nocturnal marine atmosphere. As a consequence, unlike the demonstrated effect
21 of iodine on the levels of daytime oxidants, the impact of active iodine upon the main nighttime
22 oxidant, NO₃, remains an open question. This is important given that in many parts of the ocean
23 the NO₃ + DMS reaction is at least as important as OH + DMS in oxidizing DMS (Allan et al.,

1 2000), and hence a reduction of NO₃ may have an effect in the production of SO₂ and methane
2 sulfonic acid (MSA). Here, we discuss possible mechanisms of nighttime iodine radical
3 activation and their potential effect on nighttime iodine ocean fluxes and the currently modeled
4 dawn spike in IO. A new reaction of HOI with NO₃ is proposed, supported by theoretical
5 calculations. We explore the implications of this new reaction both for iodine and NO₃
6 chemistries.

7

8 **2. Nocturnal iodine radical activation mechanism**

9 We use the reaction mechanism that has recently been described in the global modelling studies
10 by Saiz-Lopez et al. (2014) and (Ordóñez et al., 2012) (see supplementary information). In
11 addition to the reactions included in that scheme, we also include nighttime gas-phase reactions
12 based on the theoretical calculations described below. The additional reactions are listed in Table
13 1 and a scheme with this new nocturnal chemistry is included in Figure 1.

14 To the best of our knowledge, reactions of HOI specific to night time have not been studied,
15 either theoretically or through laboratory experiments. Currently, HOI is thought to build up
16 overnight until sunrise, with only heterogeneous uptake on seasalt aerosol as a nighttime loss
17 process (Saiz-Lopez et al., 2012b; Simpson et al., 2015). In addition to the well known I₂ + NO₃
18 reaction (R1) (Chambers et al., 1992), here we consider several possible HOI reactions that could
19 occur at night, in the absence of photolysis and OH:





2

3 **3. Theoretical calculations**

4 In order to explore the feasibility of reactions 2–4 taking place under the conditions of the lower
5 troposphere, we carried out electronic structure calculations using the hybrid density
6 functional/Hartree-Fock B3LYP method from within the Gaussian 09 suite of programs (Frisch
7 et al., 2009), combined with a G2 level basis set for I (Glukhovtsev et al., 1995) and the standard
8 6-311+g(2d,p) triple zeta basis set for O, N and H. Following geometry optimizations of the
9 relevant points on the potential energy surfaces, and the determination of their corresponding
10 vibrational frequencies and (harmonic) zero-point energies, energies relative to the reactants
11 were obtained at the same level of theory. Spin-orbit corrections of -30.0 (Mečiarová et al.,
12 2011), -14.4 (Khanniche et al., 2016), -5.9 (Šulková et al., 2013) and -4.8 (Kaltsoyannis and
13 Plane, 2008) kJ mol^{-1} were applied to the energies of I, IO, HOI and IONO_2 , respectively.

14 Reaction 2 is endothermic by 2.6 kJ mol^{-1} and so, within the expected error of $\pm 10 \text{ kJ mol}^{-1}$ at
15 this level of theory, might be reasonably fast. However, the transition state of the reaction, which
16 is illustrated in Figure 2(a), is 73 kJ mol^{-1} above the reactants and so this reaction will not occur
17 at tropospheric temperatures. Reaction 3 is exothermic by 19.8 kJ mol^{-1} . An HOI-- HNO_3
18 complex first forms (Figure 2(b)), which is 21 kJ mol^{-1} below the reactants. However, this
19 complex re-arranges to the $\text{IONO}_2 + \text{H}_2\text{O}$ products via the cyclic transition state shown in Figure
20 2(c), which is 110 kJ mol^{-1} above the reactants.

21 The stationary points on the potential energy surface (PES) for reaction 4 are illustrated in Figure
22 3. HOI and NO_3 associate to form a complex which is 24 kJ mol^{-1} below the reactant entrance

1 channel. H-atom transfer involves a submerged transition state to form an IO--HNO₃ complex,
2 which can then dissociate to the products IO + HNO₃. The vibrational frequencies, rotational
3 energies and geometries (in Cartesian co-ordinates) of these intermediates are listed in Table 2.
4 Overall, the reaction is exothermic by 14 kJ mol⁻¹. The energies of the HOI--NO₃ complex and
5 the transition state are assigned the same spin-orbit correction as HOI (-5.9 kJ mol⁻¹ (Šulková et
6 al., 2013)), whereas the IO--HNO₃ complex is assigned the spin-orbit correction of IO (-14.4 kJ
7 mol⁻¹ (Khanniche et al., 2016)). This reflects the H-OI bond only increasing from 0.97 Å in HOI
8 to 1.1 Å in the transition state, compared with 1.7 Å in the IO—HNO₃ complex. The spin-orbit
9 correction for the transition state is therefore likely to be closer to that of HOI. Assigning the
10 HOI spin-orbit correction therefore means that the barrier is highest with respect to the reactants,
11 so that the estimated rate coefficient (see below) may be a lower limit.

12 The rate coefficient for reaction 4 was then estimated using Rice-Ramsperger-Kassel-Markus
13 (RRKM) theory, employing a multi-well energy-grained master equation solver based on the
14 inverse Laplace transform method - MESMER (Master Equation Solver for Multi-well Energy
15 Reactions) (Roberston et al., 2014). The reaction proceeds via the formation of the excited
16 HOI--NO₃ complex from HOI + NO₃. This complex can then dissociate back to the reactants or
17 rearrange to the IO--HNO₃ intermediate complex over the transition state, which can in turn
18 dissociate to the products IO + HNO₃. Either of the intermediates can also be stabilized by
19 collision with the third body (N₂). The time evolution of all these possible outcomes is modelled
20 using the master equation.

21 The internal energies of the intermediates on the PES were divided into a contiguous set of
22 grains (width 10 cm⁻¹), each containing a bundle of rovibrational states calculated with the
23 molecular parameters in Table 2, using the rigid-rotor harmonic oscillator approximation for all

1 species. It should be noted that the HOI--NO₃ and IO--HNO₃ complexes both have low
2 frequency vibrational modes ($< 100 \text{ cm}^{-1}$) which should more correctly be treated as hindered
3 rotors rather than vibrations. However, in our experience this is not worth doing this until
4 experimental rate coefficients are available to fit the rotor barrier heights. In any case, the
5 energies of both complexes are far enough below the energy of the entrance channel (figure 3)
6 that relatively small changes in their densities of states will have a minor effect on the overall
7 rate coefficient. Each grain was then assigned a set of microcanonical rate coefficients linking it
8 to other intermediates, calculated by RRKM theory. For dissociation to products or reactants,
9 microcanonical rate coefficients were determined using inverse Laplace transformation to link
10 them directly to the capture rate coefficient, k_{capture} . For reaction 4 and the reverse reaction IO +
11 HNO₃ involving neutral species, k_{capture} was set to a typical capture rate coefficient of 2.5×10^{-10}
12 $(T/300 \text{ K})^{1/6} \text{ cm}^3 \text{ molecule}^{-1} \text{ s}^{-1}$, where the small positive temperature dependence is
13 characteristic of a long-range potential governed by dispersion and dipole-dipole forces
14 (Georgievskii and Klippenstein, 2005).

15 The probability of collisional transfer between grains was estimated using the exponential down
16 model, where the average energy for downward transitions was set to $\langle \Delta E \rangle_{\text{down}} = 300 \text{ cm}^{-1}$ for
17 N₂ as the third body (Gilbert and Smith, 1990). MESMER determines the temperature- and
18 pressure-dependent rate coefficient from the full microcanonical description of the system time
19 evolution by performing an eigenvector/eigenvalue analysis (Bartis and Widom, 1974). The
20 resulting rate coefficient over the temperature range 260 - 300 K at a pressure of 1000 hPa is
21 $k_4(T) = 2.7 \times 10^{-12} (300 \text{ K} / T)^{2.66} \text{ cm}^3 \text{ molecule}^{-1} \text{ s}^{-1}$. Because the intermediate complexes are
22 not strongly bound, and the transition state and products are below the entrance channel, the only
23 products formed in reaction R4 under atmospheric conditions are IO + HNO₃. The uncertainty in

1 k_4 arises principally from the estimated capture rate coefficient (see above), and the height of the
2 barrier below the entrance channel. As discussed above, the spin-orbit correction of the transition
3 state is likely to be larger than the value of -5.9 kJ mol^{-1} corresponding to HOI, so k_4 is possibly a
4 lower limit. For instance, if the barrier height is decreased by 3 kJ mol^{-1} , k_4 increases by a factor
5 of 1.9. If the barrier is lower by 8.5 kJ mol^{-1} (corresponding to the transition state having the
6 same spin-orbit correction as IO), then k_4 would increase by a factor of 5.1. Nevertheless, noting
7 that the capture rate coefficient could be lower – perhaps by a factor of 2 - than the estimate used
8 here, we prefer to use the value for k_4 calculated with the potential surface in Figure 3. Of course,
9 if k_4 is larger, then the atmospheric impacts of reaction 4 discussed in Section 4 will be even
10 more pronounced.

11 Note that NO_3 also reacts with CH_2I_2 with a rate constant $\sim 2\text{-}4 \times 10^{-13} \text{ cm}^3 \text{ molecule}^{-1} \text{ s}^{-1}$, which
12 can have a significant effect on nighttime CH_2I_2 concentration (Carpenter et al., 2015). However
13 the products of this reaction are still uncertain (Nakano et al., 2006; Carpenter et al., 2015) and
14 its rate is considerably slower than that of R4.

15 In summary, the only likely gas-phase reactions that I_2 and HOI undergo in the nighttime
16 troposphere are R1 and R4, respectively. These are included in the model reaction scheme to
17 examine their impacts on the evolution of iodine species in the atmosphere.

18

19 **4. Atmospheric modelling**

20 We use two atmospheric chemical transport models to study *i*) the impact of this new chemistry
21 on the nighttime chemistry and partitioning of iodine species, and *ii*) the resulting geographical
22 distribution of nocturnal iodine and impact on NO_3 within the global marine boundary layer.

1 The first model, Tropospheric HAlogen chemistry MOdel (THAMO), is used for a detailed
2 kinetics study of the impact of the different reactions shown in Table 1 as well as to assess which
3 uptake rates best reproduce observations from a field study at the CVAO (Carpenter et al., 2011).
4 THAMO has been used in the past to study iodine chemistry at the CVAO and further details
5 including the full chemical scheme can be found elsewhere (Read et al., 2008; Saiz-Lopez et al.,
6 2008; Mahajan et al., 2009; Mahajan et al., 2010a; Mahajan et al., 2010b; Lawler et al., 2014).
7 Briefly, THAMO is a 1-D chemistry transport model with 200 stacked boxes at a vertical
8 resolution of 5m (total height 1 km). The model treats iodine, bromine, O₃, NO_x and HO_x
9 chemistry, and is constrained with typical measured values of other chemical species in the
10 MBL: [CO]=110 nmol mol⁻¹; [DMS]=30 pmol/mol; [CH₄]=1820 nmol mol⁻¹; [ethane]=925
11 pmol/mol; [CH₃CHO]=970 pmol/mol; [HCHO]=500 pmol/mol; [isoprene]=10 pmol/mol;
12 [propane]=60 pmol/mol; [propene]=20 pmol/mol. The average background aerosol surface area
13 (ASA) used is 1x10⁻⁶ cm² cm⁻³ (Read et al., 2008; Lee et al., 2009; Read et al., 2009; Lee et al.,
14 2010). The model is initialized at midnight and the evolution of iodine species, O₃, NO_x and HO_x
15 is followed until the model reaches steady state.

16 The second model is the global 3D chemistry-climate model CAM-Chem (Community
17 Atmospheric Model with chemistry, version 4.0), which is used to study the impact of reactions
18 1 and 4 on a global scale. The model includes a comprehensive chemistry scheme to simulate the
19 evolution of trace gases and aerosols in the troposphere and the stratosphere (Lamarque et al.,
20 2012). The model runs with the iodine and bromine chemistry schemes from previous studies
21 (Fernandez et al., 2014; Saiz-Lopez et al., 2014; Saiz-Lopez et al., 2015), including the
22 photochemical breakdown of bromo- and iodo-carbons emitted from the oceans (Ordóñez et al.,
23 2012) and abiotic oceanic sources of HOI and I₂ (Prados-Roman et al., 2015a). CAM-Chem has

1 been configured in this work with a horizontal resolution of 1.9° latitude by 2.5° longitude and 26
2 vertical levels, from the surface to ~40km altitude. All model runs in this study were performed
3 in the specified dynamics mode (Lamarque et al., 2012) using offline meteorological fields
4 instead of an online calculation, to allow direct comparisons between different simulations. This
5 offline meteorology consists of a high frequency meteorological input from a previous free
6 running climatic simulation.

7 It should be noted that during nighttime the uptake on aerosols of emitted species such as I₂ and
8 HOI, and the uptake of reservoir species such as IONO₂, can play a major role in the cycling of
9 iodine. Observations at CVAO show that I₂ peaked at about 1 pmol/mol during the night and that
10 ICl was not detected above the 1 pmol/mol detection limit of the instrument (Lawler et al.,
11 2014). In order to match these observations, we need to reduce the uptake and heterogeneous
12 recycling of iodine species. The uptake rates of chemical species on the background seasalt
13 aerosols are determined by their uptake coefficients (γ). The database of mass accommodation
14 and/or uptake coefficients is rather sparse and essentially limited to I₂, HI, HOI, ICI, IBr on pure
15 water/ice and on sulphuric acid particles (Sander et al., 2006). Other iodine species which are
16 likely to undergo uptake onto aerosol are OIO, HIO₃, IONO₂, IONO₂, I₂O₂ (Saiz-Lopez et al.,
17 2012a; Sommariva et al., 2012). Uptake of HOI is very uncertain, with γ (HOI) ranging from $2 \times$
18 10^{-3} to 0.3 depending on the surface composition and state (Holmes et al., 2001). Sommariva et
19 al. (2012) assumed γ (HOI) to be 0.6, similar to the value for HOBr measured by Wachsmuth et
20 al. (2002). In the case of IONO₂, the uptake coefficient has not been measured, with most models
21 using values of 0.1 (von Glasow et al., 2002; Saiz-Lopez et al., 2008; Mahajan et al., 2009; Leigh
22 et al., 2010; Mahajan et al., 2010a; Mahajan et al., 2010b; Sommariva et al., 2012; Lawler et al.,
23 2014). The modelled levels of I₂ and ICl change with different values of uptake coefficients. To

1 match the CVAO I₂ and ICl observations (Lawler et al., 2014), we have used $\gamma = 0.01$ for HOI
2 and IONO₂, which is within the uncertainty in the literature, and assumed that 80% is recycled as
3 I₂. Further measurements of these dihalogen species are needed to better constrain their
4 heterogeneous recycling on seasalt aerosols.

5

6 **5. Results and discussion**

7 Of the possible nocturnal iodine activation reactions involving the inorganic iodine source gases
8 I₂ and HOI, only reactions R1 and R4 appear to be likely candidates (see Section 3). We
9 therefore designed two modelling scenarios: Scenario 1 (S1), without nighttime reactions of I₂ or
10 HOI with NO₃; and Scenario 2 (S2), including reactions R1 and R4 for the degradation of HOI
11 and I₂ by NO₃. In the one-dimensional model THAMO, the I₂ and HOI are injected into the
12 atmosphere from the ocean surface using the flux parameterizations derived from laboratory
13 experiments (Carpenter et al., 2013; MacDonald et al., 2014). Figure 4 shows the resulting
14 diurnal evolution of the HOI and I₂ mixing ratios in the two scenarios, after two days of
15 simulation time. The I₂ mixing ratio peaks during the night in both the scenarios due to quick
16 loss by photolysis during the daytime. By contrast, HOI is present during daytime due to its
17 production through the reaction of IO with HO₂, and peaks just before sunset. In the first
18 scenario, without the inclusion of reactions R1 and R4, Figure 4 (right-hand side panels) shows
19 that I₂ build up during the night, reaching a concentration peak just before dawn. This is
20 especially noticeable as the daytime concentrations are much lower than during the night. On the
21 other hand, HOI concentrations decrease during night until dawn, when they drop to zero. For
22 both species, inclusion of reactions with NO₃ causes a decrease in their respective nocturnal

1 concentrations (Fig. 4, left-hand side panels). The inclusion of reactions R1 and R4 also leads to
2 a modelled I_2 concentration which is in better agreement with the observations of the molecule
3 made at CVAO (Lawler et al., 2014), reaching peak values of about 1 pmol/mol, as compared to
4 about 3 pmol/mol for the scenario without nighttime reactions. An additional consequence of
5 including reactions R1 and R4 is the significant increase of the sea-air fluxes of HOI and I_2 at
6 night due to their atmospheric removal by NO_3 (Fig. 4, bottom panel).

7 Figure 5 shows the diurnal evolution of IO, NO_3 and $IONO_2$ in both model scenarios after two
8 days of simulation time. Although the daytime peak values of IO are well reproduced in both
9 scenarios, reaching about 1.5 pmol/mol around noon similar to the ground-based observations
10 (Read et al., 2008), the inclusion of reactions R1 and R4 leads to the removal of the dawn spike
11 in IO, which is predicted by current iodine models but was not observed at CVAO (Read et al.,
12 2008; Mahajan et al., 2010a). The IO dawn spike predicted by models is due to a buildup of the
13 emitted I_2 and HOI (which is converted into IBr/ICl through heterogeneous recycling) over the
14 night, followed by rapid photolysis after first sunlight. However, due to the considerable removal
15 of HOI and I_2 through the night due to reaction with ambient NO_3 , this spike does not appear in
16 the second scenario, leading to a modification of the diurnal profile of IO that better matches
17 with observations.

18 Reactions R1 and R4 also reduce the NO_3 mixing ratio (Fig. 5, middle panels). In scenario 1, the
19 NO_3 is modelled to peak at about 14 pmol/mol just before dawn. However, the inclusion of
20 reactions R1 and R4 leads to near complete depletion of NO_3 close to the surface, with the peak
21 level at the surface reaching only 2 pmol/mol, since reactions R1 and R4 become the main
22 atmospheric loss processes for NO_3 in the lower MBL. These reactions lead however to the
23 buildup of $IONO_2$ during the night (Fig. 5, bottom panels). In the absence of reactions R1 and

1 R4, significant levels of IONO₂ are seen only at dawn and dusk since no other reactions produce
2 IONO₂ at night, and during the day IONO₂ is removed by photolysis. However, with continuous
3 conversion of I₂ and HOI to IONO₂ by reactions R1 and R4 in scenario 2, IONO₂ is modelled to
4 reach up to 3 pmol/mol in the nocturnal MBL.

5 Given the associated uncertainty in the theoretical estimate of the k_4 , we used THAMO to assess
6 the sensitivity of surface NO₃ to k_4 . Figure 6 shows that NO₃ peak nighttime concentration is in
7 fact highly coupled to k_4 , with the expected uncertainty in k_4 of one order of magnitude (see
8 above) giving rise to a factor of two change in NO₃. A laboratory measurement of k_4 should
9 therefore be undertaken in the future.

10 We now implement the nighttime reactions in the 3D global model (CAM-Chem) to assess the
11 resulting geographical distributions and impacts of these reactions. We have also run two
12 different scenarios in CAM-Chem, the first without R1 and R4 in the chemical scheme, and the
13 second including the new nighttime iodine chemistry. Figure 7 shows how the inclusion of R1
14 and R4 reduces globally the nighttime concentrations of I₂ and HOI. The plots correspond to the
15 nighttime averaged (from 00LT to 01LT (Local Time)) differences between the model scenarios.
16 Considerable reductions of up to 0.5 and 10 pmol/mol (i.e. up to 100% removal) are observed for
17 I₂ and HOI, respectively, particularly over coastal polluted regions where continental pollution
18 outflow leads to higher levels of NO₃ in the nighttime MBL. Major shipping routes also show
19 strong nocturnal iodine activity due to the characteristically high NO_x, and resulting NO₃,
20 associated with shipping emissions.

21 Figure 8 shows the effect of this nocturnal chemistry on the concentrations of IONO₂ and NO₃.
22 As in the previous figure, the plots correspond to the nighttime averaged difference between the

1 second and the first scenarios. The maps show an increase of IONO₂ of up to 15 pmol/mol
2 (~600%) over polluted coastal areas, due to efficient conversion of NO₃ into IONO₂. The bottom
3 panel of Figure 7 shows the expected decrease of NO₃ levels associated with the inclusion of
4 reactions R1 and R4, with decreases of up to ~4 pmol/mol (up to 60%) over marine polluted
5 regions. We model global percentage reductions in the NO₃ concentrations of 7.1% (60S-60N),
6 with nitrate removal of up to 80% in non-polluted remote oceanic regions with low NO₃ levels.
7 This in turn can affect the modelled oxidation of DMS by NO₃. We estimate that the reduction in
8 NO₃, due to the inclusion of R1 and R4, results in a model increase in DMS levels of up to 7
9 pmol/mol (about 20%) in marine regions affected by continental pollution outflow (Fig. 9). We
10 therefore suggest that the inclusion of the new nighttime iodine chemistry can have a large, so far
11 unrecognized, impact on the nocturnal oxidizing capacity of the marine atmosphere.

12 The hourly evolution of the main species involved in this study is shown in Figures 10 and 11,
13 which include the levels of HOI, I₂, IONO₂ and NO₃ in the MBL over regions where nocturnal
14 iodine is modelled to be particularly active. The first region is located within the Mediterranean
15 Sea, an area that shows large differences during the summer months when high ozone levels
16 drive large emissions of HOI and I₂ from the sea, and the high levels of NO₃ at nighttime make
17 this chemistry especially important. The hourly average in August is shown in Figure 10 for
18 HOI, IONO₂ and I₂. HOI and IONO₂ (Fig 10) are the species whose concentration differ most
19 between scenarios as HOI is removed and IONO₂ produced by R4 (and, to a lesser extent, R1).
20 Over a Pacific Ocean region at the south of the Baja California Peninsula, the modelled
21 differences between the two scenarios are even higher than over the Mediterranean Sea (Figure
22 11). Large differences in MBL NO₃, up to 28%, are modelled during the night caused by
23 pollution outflow from the west coasts of Mexico and USA.

1

2 **6. Summary and conclusions**

3 The viability of the reaction of HOI with NO₂, HNO₃ and NO₃ has been studied by theoretical
4 calculations. The results indicate that only the reaction of HOI with NO₃, to yield IO + HNO₃, is
5 possible under tropospheric conditions. The inclusion of this reaction, along with that of I₂ +
6 NO₃, has a number of significant implications: *i*) nocturnal iodine radical chemistry is activated;
7 *ii*) this causes enhanced nighttime oceanic emissions of HOI and I₂; *iii*) nighttime iodine species
8 are partitioned into high levels of IONO₂; *iv*) the IO spike, modelled by current iodine models
9 but not shown by observations, is removed; and, *v*) a reduction of the levels of nitrate radical in
10 the MBL, with the associated less efficient oxidation of DMS, which has important implications
11 for our understanding of the nocturnal oxidizing capacity of the marine atmosphere.

12

13

14 **Acknowledgments**

15 This work was supported by the Spanish National Research Council (CSIC). The National
16 Center for Atmospheric Research (NCAR) is funded by the National Science Foundation NSF.
17 The Climate Simulation Laboratory at NCAR's Computational and Information Systems
18 Laboratory (CISL) provided the computing resources (ark:/85065/d7wd3xhc). As part of the
19 CESM project, CAM-Chem is supported by the NSF and the Office of Science (BER) of the US
20 Department of Energy. This work was also sponsored by the NASA Atmospheric Composition
21 Modeling and Analysis Program Activities (ACMAP, number NNX11AH90G).

1

2 **References**

3 Allan, B. J., McFiggans, G., Plane, J. M. C., Coe, H., and McFadyen, G. G.: The nitrate radical
4 in the remote marine boundary layer, *Journal of Geophysical Research: Atmospheres*, 105,
5 24191-24204, 10.1029/2000jd900314, 2000.

6 Allan, J. D., Williams, P. I., Najera, J., Whitehead, J. D., Flynn, M. J., Taylor, J. W., Liu, D.,
7 Darbyshire, E., Carpenter, L. J., Chance, R., Andrews, S. J., Hackenberg, S. C., and McFiggans,
8 G.: Iodine observed in new particle formation events in the Arctic atmosphere during
9 ACCACIA, *Atmos. Chem. Phys.*, 15, 5599-5609, 10.5194/acp-15-5599-2015, 2015.

10 Bartis, J. T., and Widom, B.: Stochastic models of the interconversion of three or more chemical
11 species, *J. Chem. Phys.*, 60, 3474-3482, doi: 10.1063/1.1681562, 1974.

12 Butler, J. H., King, D. B., Lobert, J. M., Montzka, S. A., Yvon-Lewis, S. A., Hall, B. D.,
13 Warwick, N. J., Mondeel, D. J., Aydin, M., and Elkins, J. W.: Oceanic distributions and
14 emissions of short-lived halocarbons, *Global Biogeochem. Cycles*, 21, GB1023,
15 10.1029/2006gb002732, 2007.

16 Carpenter, L. J.: Iodine In the marine Boundary Layer, *Chem. Rev.*, 103 (12), 4953-4962, 2003.

17 Carpenter, L. J., Fleming, Z. L., Read, K. A., Lee, J. D., Moller, S. J., Hopkins, J. R., Purvis, R.
18 M., Lewis, A. C., Müller, K., Heinold, B., Herrmann, H., Fomba, K. W., Pinxteren, D., Müller,
19 C., Tegen, I., Wiedensohler, A., Müller, T., Niedermeier, N., Achterberg, E. P., Patey, M. D.,
20 Kozlova, E. A., Heimann, M., Heard, D. E., Plane, J. M. C., Mahajan, A., Oetjen, H., Ingham, T.,
21 Stone, D., Whalley, L. K., Evans, M. J., Pilling, M. J., Leigh, R. J., Monks, P. S., Karunaharan,

1 A., Vaughan, S., Arnold, S. R., Tschritter, J., Pöhler, D., Frieß, U., Holla, R., Mendes, L. M.,
2 Lopez, H., Faria, B., Manning, A. J., and Wallace, D. W. R.: Seasonal characteristics of tropical
3 marine boundary layer air measured at the Cape Verde Atmospheric Observatory, *J. Atmos.*
4 *Chem.*, 67, 87-140, 10.1007/s10874-011-9206-1, 2011.

5 Carpenter, L. J., MacDonald, S. M., Shaw, M. D., Kumar, R., Saunders, R. W., Parthipan, R.,
6 Wilson, J., and Plane, J. M. C.: Atmospheric iodine levels influenced by sea surface emissions of
7 inorganic iodine, *Nature Geosci*, 6, 108-111, 10.1038/ngeo1687, 2013.

8 Carpenter, L. J., Andrews, S. J., Lidster, R. T., Saiz-Lopez, A., Fernandez-Sanchez, M., Bloss,
9 W. J., Ouyang, B., and Jones, R. L.: A nocturnal atmospheric loss of
10 CH_2I_2 in the remote marine boundary layer, *J. Atmos. Chem.*,
11 10.1007/s10874-015-9320-6, 2015.

12 Fernandez, R. P., Salawitch, R. J., Kinnison, D. E., Lamarque, J. F., and Saiz-Lopez, A.:
13 Bromine partitioning in the tropical tropopause layer: implications for stratospheric injection,
14 *Atmos. Chem. Phys.*, 14, 13391-13410, 10.5194/acp-14-13391-2014, 2014.

15 Frisch, M., Trucks, G., Schlegel, H., Scuseria, G., Robb, M., Cheeseman, J., Scalmani, G.,
16 Barone, V., Mennucci, B., and Petersson, G.: Gaussian 09, Revision A. 1. Wallingford, CT:
17 Gaussian, Inc, 2009.

18 Georgievskii, Y., and Klippenstein, S. J.: Long-range transition state theory, *J. Chem. Phys.*, 122,
19 194103, doi: 10.1063/1.1899603, 2005.

20 Gilbert, R. G., and Smith, S. C.: *Theory of Unimolecular and Recombination Reactions*,
21 Blackwell, Oxford, 1990.

1 Glukhovtsev, M. N., Pross, A., McGrath, M. P., and Radom, L.: Extension of Gaussian-2 (G2)
2 theory to bromine- and iodine-containing molecules: Use of effective core potentials, *J. Chem.*
3 *Phys.*, 103, 1878-1885, 1995.

4 Gomez Martin, J. C., Galvez, O., Baeza-Romero, M. T., Ingham, T., Plane, J. M. C., and Blitz,
5 M. A.: On the mechanism of iodine oxide particle formation, *Phys. Chem. Chem. Phys.*, 15,
6 15612-15622, 10.1039/c3cp51217g, 2013.

7 Gómez Martín, J. C., Mahajan, A. S., Hay, T. D., Prados-Román, C., Ordóñez, C., MacDonald,
8 S. M., Plane, J. M. C., Sorribas, M., Gil, M., Paredes Mora, J. F., Agama Reyes, M. V., Oram, D.
9 E., Leedham, E., and Saiz-Lopez, A.: Iodine chemistry in the eastern Pacific marine boundary
10 layer, *Journal of Geophysical Research: Atmospheres*, 118, 887-904, 10.1002/jgrd.50132, 2013.

11 Großmann, K., Frieß, U., Peters, E., Wittrock, F., Lampel, J., Yilmaz, S., Tschritter, J.,
12 Sommariva, R., von Glasow, R., Quack, B., Krüger, K., Pfeilsticker, K., and Platt, U.: Iodine
13 monoxide in the Western Pacific marine boundary layer, *Atmos. Chem. Phys.*, 13, 3363-3378,
14 10.5194/acp-13-3363-2013, 2013.

15 Hoffmann, T., O'Dowd, C. D., and Seinfeld, J. H.: Iodine oxide homogeneous nucleation: An
16 explanation for coastal new particle production, *Geophys. Res. Lett.*, 28, 1949-1952, 2001.

17 Holmes, N. S., Adams, J. W., and Crowley, J. N.: Uptake and reaction of HOI and IONO₂ on
18 frozen and dry NaCl/NaBr surfaces and H₂SO₄, *Phys. Chem. Chem. Phys.*, 3, 1679-1687,
19 10.1039/b100247n, 2001.

1 Jones, C. E., Hornsby, K. E., Sommariva, R., Dunk, R. M., von Glasow, R., McFiggans, G., and
2 Carpenter, L. J.: Quantifying the contribution of marine organic gases to atmospheric iodine,
3 *Geophys. Res. Lett.*, 37, L18804, 2010.

4 Kaltsoyannis, N., and Plane, J. M. C.: Quantum chemical calculations on a selection of iodine-
5 containing species (IO, OIO, INO_3 , $(\text{IO})_2$, I_2O_3 , I_2O_4 and I_2O_5) of importance in the atmosphere.,
6 *Phys. Chem. Chem. Phys.*, 10, 1723-1733, 2008.

7 Khanniche, S., Louis, F., Cantrel, L., and Černušák, I.: A Density Functional Theory and ab
8 Initio Investigation of the Oxidation Reaction of CO by IO Radicals, *J. Phys. Chem. A*, 120,
9 1737–1749, 2016.

10 Lamarque, J. F., Emmons, L. K., Hess, P. G., Kinnison, D. E., Tilmes, S., Vitt, F., Heald, C. L.,
11 Holland, E. A., Lauritzen, P. H., Neu, J., Orlando, J. J., Rasch, P. J., and Tyndall, G. K.: CAM-
12 chem: description and evaluation of interactive atmospheric chemistry in the Community Earth
13 System Model, *Geosci. Model Dev.*, 5, 369-411, 10.5194/gmd-5-369-2012, 2012.

14 Lawler, M. J., Mahajan, A. S., Saiz-Lopez, A., and Saltzman, E. S.: Observations of I_2 at a
15 remote marine site, *Atmos. Chem. Phys.*, 14, 2669-2678, 10.5194/acp-14-2669-2014, 2014.

16 Lee, J. D., Moller, S. J., Read, K. A., Lewis, A. C., Mendes, L., and Carpenter, L. J.: Year-round
17 measurements of nitrogen oxides and ozone in the tropical North Atlantic marine boundary layer,
18 *Journal of Geophysical Research: Atmospheres*, 114, n/a-n/a, 10.1029/2009jd011878, 2009.

19 Lee, J. D., McFiggans, G., Allan, J. D., Baker, A. R., Ball, S. M., Benton, A. K., Carpenter, L. J.,
20 Commane, R., Finley, B. D., Evans, M., Fuentes, E., Furneaux, K., Goddard, A., Good, N.,
21 Hamilton, J. F., Heard, D. E., Herrmann, H., Hollingsworth, A., Hopkins, J. R., Ingham, T.,

1 Irwin, M., Jones, C. E., Jones, R. L., Keene, W. C., Lawler, M. J., Lehmann, S., Lewis, A. C.,
2 Long, M. S., Mahajan, A., Methven, J., Moller, S. J., Müller, K., Müller, T., Niedermeier, N.,
3 O'Doherty, S., Oetjen, H., Plane, J. M. C., Pszenny, A. A. P., Read, K. A., Saiz-Lopez, A.,
4 Saltzman, E. S., Sander, R., von Glasow, R., Whalley, L., Wiedensohler, A., and Young, D.:
5 Reactive Halogens in the Marine Boundary Layer (RHAMBLe): the tropical North Atlantic
6 experiments, *Atmos. Chem. Phys.*, 10, 1031-1055, 10.5194/acp-10-1031-2010, 2010.

7 Leigh, R. J., Ball, S. M., Whitehead, J., Leblanc, C., Shillings, A. J. L., Mahajan, A. S., Oetjen,
8 H., Dorsey, J. R., Gallagher, M., Jones, R. L., Plane, J. M. C., Potin, P., and McFiggans, G.:
9 Measurements and modelling of molecular iodine emissions, transport and photodestruction in
10 the coastal region around Roscoff, *Atmos. Chem. Phys.*, 10, 11823-11838, 2010.

11 MacDonald, S. M., Gómez Martín, J. C., Chance, R., Warriner, S., Saiz-Lopez, A., Carpenter, L.
12 J., and Plane, J. M. C.: A laboratory characterisation of inorganic iodine emissions from the sea
13 surface: dependence on oceanic variables and parameterisation for global modelling, *Atmos.*
14 *Chem. Phys.*, 14, 5841-5852, 10.5194/acp-14-5841-2014, 2014.

15 Mahajan, A. S., Oetjen, H., Saiz-Lopez, A., Lee, J. D., McFiggans, G. B., and Plane, J. M. C.:
16 Reactive iodine species in a semi-polluted environment, *Geophys. Res. Lett.*, 36, L16803,
17 doi:16810.11029/12009GL038018, 2009.

18 Mahajan, A. S., Plane, J. M. C., Oetjen, H., Mendes, L., Saunders, R. W., Saiz-Lopez, A., Jones,
19 C. E., Carpenter, L. J., and McFiggans, G. B.: Measurement and modelling of tropospheric
20 reactive halogen species over the tropical Atlantic Ocean, *Atmos. Chem. Phys.*, 10, 4611-4624,
21 2010a.

1 Mahajan, A. S., Shaw, M., Oetjen, H., Hornsby, K. E., Carpenter, L. J., Kaleschke, L., Tian-
2 Kunze, X., Lee, J. D., Moller, S. J., Edwards, P., Commane, R., Ingham, T., Heard, D. E., and
3 Plane, J. M. C.: Evidence of reactive iodine chemistry in the Arctic boundary layer, *J. Geophys.*
4 *Res.*, [Atmos.], 115, D20303, doi:10.1029/2009JD013665, 2010b.

5 Mahajan, A. S., Gómez Martín, J. C., Hay, T. D., Royer, S. J., Yvon-Lewis, S., Liu, Y., Hu, L.,
6 Prados-Roman, C., Ordóñez, C., Plane, J. M. C., and Saiz-Lopez, A.: Latitudinal distribution of
7 reactive iodine in the Eastern Pacific and its link to open ocean sources, *Atmos. Chem. Phys.*, 12,
8 11609-11617, 10.5194/acp-12-11609-2012, 2012.

9 McFiggans, G., Coe, H., Burgess, R., Allan, J., Cubison, M., Alfarra, M. R., Saunders, R., Saiz-
10 Lopez, A., Plane, J. M. C., Wevill, D. J., Carpenter, L. J., Rickard, A. R., and Monks, P. S.:
11 Direct evidence for coastal iodine particles from *Laminaria* macroalgae - linkage to emissions of
12 molecular iodine, *Atmos. Chem. Phys.*, 4, 701-713, 2004.

13 Mečiarová, K., Šulka, M., Canneaux, S., Louis, F., and Černušáka, I.: A theoretical study of the
14 kinetics of the forward and reverse reactions $\text{HI} + \text{CH}_3 = \text{I} + \text{CH}_4$, *Chem. Phys. Lett.*, 517, 149-
15 154, 2011.

16 Nakano, Y., Ukeguchi, H., and Ishiwata, T.: Rate constant of the reaction of NO_3 with CH_2I_2
17 measured with use of cavity ring-down spectroscopy, *Chem. Phys. Lett.*, 430, 235-239, doi:
18 10.1016/j.cplett.2006.09.002, 2006.

19 O'Dowd, C. D., Jimenez, J. L., Bahreini, R., Flagan, R. C., Seinfeld, J. H., Hameri, K., Pirjola,
20 L., Kulmala, M., Jennings, S. G., and Hoffmann, T.: Marine aerosol formation from biogenic
21 iodine emissions, *Nature*, 417, 632-636, 2002.

1 Ordóñez, C., Lamarque, J. F., Tilmes, S., Kinnison, D. E., Atlas, E. L., Blake, D. R., Sousa
2 Santos, G., Brasseur, G., and Saiz-Lopez, A.: Bromine and iodine chemistry in a global
3 chemistry-climate model: description and evaluation of very short-lived oceanic sources, *Atmos.*
4 *Chem. Phys.*, 12, 1423-1447, 10.5194/acp-12-1423-2012, 2012.

5 Prados-Roman, C., Cuevas, C. A., Fernandez, R. P., Kinnison, D. E., Lamarque, J. F., and Saiz-
6 Lopez, A.: A negative feedback between anthropogenic ozone pollution and enhanced ocean
7 emissions of iodine, *Atmos. Chem. Phys.*, 15, 2215-2224, 10.5194/acp-15-2215-2015, 2015a.

8 Prados-Roman, C., Cuevas, C. A., Hay, T., Fernandez, R. P., Mahajan, A. S., Royer, S. J., Galí,
9 M., Simó, R., Dachs, J., Großmann, K., Kinnison, D. E., Lamarque, J. F., and Saiz-Lopez, A.:
10 Iodine oxide in the global marine boundary layer, *Atmos. Chem. Phys.*, 15, 583-593,
11 10.5194/acp-15-583-2015, 2015b.

12 Read, K. A., Mahajan, A. S., Carpenter, L. J., Evans, M. J., Faria, B. V. E., Heard, D. E.,
13 Hopkins, J. R., Lee, J. D., Moller, S. J., Lewis, A. C., Mendes, L., McQuaid, J. B., Oetjen, H.,
14 Saiz-Lopez, A., Pilling, M. J., and Plane, J. M. C.: Extensive halogen-mediated ozone
15 destruction over the tropical Atlantic Ocean, *Nature*, 453, 1232-1235, 2008.

16 Read, K. A., Lee, J. D., Lewis, A. C., Moller, S. J., Mendes, L., and Carpenter, L. J.: Intra-annual
17 cycles of NMVOC in the tropical marine boundary layer and their use for interpreting seasonal
18 variability in CO, *Journal of Geophysical Research: Atmospheres*, 114, n/a-n/a,
19 10.1029/2009jd011879, 2009.

20 Roberston, S. H., Glowacki, D. R., Liang, C. H., Morley, C., Shannon, R., Blitz, M., and Pilling,
21 M. J.: MESMER (Master Equation Solver for Multi-Energy Well Reactions), 2008–2012: An

1 object oriented C++ program for carrying out ME calculations and eigenvalue-eigenvector
2 analysis on arbitrary multiple well systems, edited. [Available at
3 <http://sourceforge.net/projects/mesmer>.], in, 4.1 ed., 2014.

4 Roscoe, H. K., Jones, A. E., Brough, N., Weller, R., Saiz-Lopez, A., Mahajan, A. S.,
5 Schoenhardt, A., Burrows, J. P., and Fleming, Z. L.: Particles and iodine compounds in coastal
6 Antarctica, *Journal of Geophysical Research: Atmospheres*, 120, 7144-7156,
7 10.1002/2015jd023301, 2015.

8 Saiz-Lopez, A., and Plane, J. M. C.: Novel iodine chemistry in the marine boundary layer,
9 *Geophys. Res. Lett.*, 31, L04112, 2004.

10 Saiz-Lopez, A., Plane, J. M. C., Mahajan, A. S., Anderson, P. S., Bauguitte, S. J.-B., Jones, A.
11 E., Roscoe, H. K., Salmon, R. A., Bloss, W. J., Lee, J. D., and Heard, D. E.: On the vertical
12 distribution of boundary layer halogens over coastal Antarctica: implications for O₃, HO_x, NO_x
13 and the Hg lifetime, *Atmos. Chem. Phys.*, 8, 887-900, 2008.

14 Saiz-Lopez, A., Lamarque, J.-F., Kinnison, D., Tilmes, S., Ordóñez, C., Orlando, J. J., Conley,
15 A. J., Plane, J. M. C., Mahajan, A., Sousa Santos, G., Atlas, E., Blake, D. R., Sander, S. P.,
16 Schauffler, S. M., Thompson, A. M., and Brasseur, G.: Estimating the climate significance of
17 halogen-driven ozone loss in the tropical marine troposphere, *Atmos. Chem. Phys.*, 12, 3939-
18 3949, 2012a.

19 Saiz-Lopez, A., Plane, J. M. C., Baker, A. R., Carpenter, L. J., Von Glasow, R., Gómez Martín,
20 J. C., McFiggans, G., and Saunders, R. W.: Atmospheric Chemistry of Iodine, *Chem. Rev.*
21 (Washington, DC, U. S.), 112, 1773-1804, 10.1021/cr200029u, 2012b.

1 Saiz-Lopez, A., Fernandez, R. P., Ordóñez, C., Kinnison, D. E., Gómez Martín, J. C., Lamarque,
2 J. F., and Tilmes, S.: Iodine chemistry in the troposphere and its effect on ozone, *Atmos. Chem.*
3 *Phys.*, 14, 13119-13143, 10.5194/acp-14-13119-2014, 2014.

4 Saiz-Lopez, A., Baidar, S., Cuevas, C. A., Koenig, T. K., Fernandez, R. P., Dix, B., Kinnison, D.
5 E., Lamarque, J. F., Rodriguez-Lloveras, X., Campos, T. L., and Volkamer, R.: Injection of
6 iodine to the stratosphere, *Geophys. Res. Lett.*, n/a-n/a, 10.1002/2015gl064796, 2015.

7 Sander, S. P., Orkin, V. L., Kurylo, M. J., Golden, D. M., Huie, R. E., Kolb, C. E., Finlayson-
8 Pitts, B. J., Molina, M. J., Friedl, R. R., Ravishankara, A. R., Moortgat, G. K., Keller-Rudek, H.,
9 and Wine, P. H.: Chemical kinetics and photochemical data for use in atmospheric studies, JPL-
10 NASA, 2006.

11 Sherwen, T., Evans, M. J., Carpenter, L. J., Andrews, S. J., Lidster, R. T., Dix, B., Koenig, T. K.,
12 Sinreich, R., Ortega, I., Volkamer, R., Saiz-Lopez, A., Prados-Roman, C., Mahajan, A. S., and
13 Ordóñez, C.: Iodine's impact on tropospheric oxidants: a global model study in GEOS-Chem,
14 *Atmos. Chem. Phys.*, 16, 1161-1186, 10.5194/acp-16-1161-2016, 2016.

15 Simpson, W. R., Brown, S. S., Saiz-Lopez, A., Thornton, J. A., and Glasow, R. v.: Tropospheric
16 Halogen Chemistry: Sources, Cycling, and Impacts, *Chem. Rev.*, 115, 4035-4062,
17 10.1021/cr5006638, 2015.

18 Sommariva, R., Bloss, W. J., and von Glasow, R.: Uncertainties in gas-phase atmospheric iodine
19 chemistry, *Atmos. Environ.*, 57, 219-232, doi: 10.1016/j.atmosenv.2012.04.032, 2012.

1 Šulková, K., Šulka, M., Louis, F., and Neogrady, P.: Atmospheric Reactivity of CH₂ICl with OH
2 Radicals: High-Level OVOS CCSD(T) Calculations for the X-Abstraction Pathways (X = H, Cl,
3 or I), *J. Phys. Chem. A*, 117, 771–782, 2013.

4 Volkamer, R., Baidar, S., Campos, T. L., Coburn, S., DiGangi, J. P., Dix, B., Eloranta, E. W.,
5 Koenig, T. K., Morley, B., Ortega, I., Pierce, B. R., Reeves, M., Sinreich, R., Wang, S., Zondlo,
6 M. A., and Romashkin, P. A.: Aircraft measurements of BrO, IO, glyoxal, NO₂, H₂O, O₂–O₂
7 and aerosol extinction profiles in the tropics: comparison with aircraft-/ship-based in situ and
8 lidar measurements, *Atmos. Meas. Tech.*, 8, 2121-2148, 10.5194/amt-8-2121-2015, 2015.

9 von Glasow, R., Sander, R., Bott, A., and Crutzen, P. J.: Modeling halogen chemistry in the
10 marine boundary layer. 1. Cloud-free MBL, *J. Geophys. Res.*, 107, 4341, 2002.

11 Wachsmuth, M., Gäggeler, H. W., von Glasow, R., and Ammann, M.: Accommodation
12 coefficient of HOBr on deliquescent sodium bromide aerosol particles, *Atmos. Chem. Phys.*, 2,
13 121-131, 10.5194/acp-2-121-2002, 2002.

14 Wang, F., Saiz-Lopez, A., Mahajan, A. S., Gómez Martín, J. C., Armstrong, D., Lemes, M., Hay,
15 T., and Prados-Roman, C.: Enhanced production of oxidised mercury over the tropical Pacific
16 Ocean: a key missing oxidation pathway, *Atmos. Chem. Phys.*, 14, 1323-1335, 10.5194/acp-14-
17 1323-2014, 2014.

18

19

1 **Tables**

2

3 Table 1: Night time reactions of emitted inorganic iodine compounds considered in addition to
 4 the iodine chemistry scheme used by (Saiz-Lopez et al., 2014).

No.	Reaction	Notes
R1.	$I_2 + NO_3 \rightarrow I + IONO_2$	$1.5 \times 10^{-12} \text{ cm}^3 \text{ molecule}^{-1} \text{ s}^{-1}$ [<i>Chambers et al.</i> , 1992]
R2.	$HOI + NO_2 \rightarrow I + HNO_3$	Endothermic by 9 kJ mol^{-1} and the transition state is 73 kJ mol^{-1} above the reactants
R3.	$HOI + HNO_3 \rightarrow IONO_2 + H_2O$	Exothermic by 11 kJ mol^{-1} . The reaction first forms a complex 21 kJ mol^{-1} below the reactants but this rearranges to the products via a transition state that is 110 kJ mol^{-1} above the reactants.
R4.	$HOI + NO_3 \rightarrow IO + HNO_3$	Exothermic by 11 kJ mol^{-1} with all transition states below the reactants. $k(T) = 2.7 \times 10^{-12} (300 \text{ K} / T)^{2.66} \text{ cm}^3 \text{ molecule}^{-1} \text{ s}^{-1}$

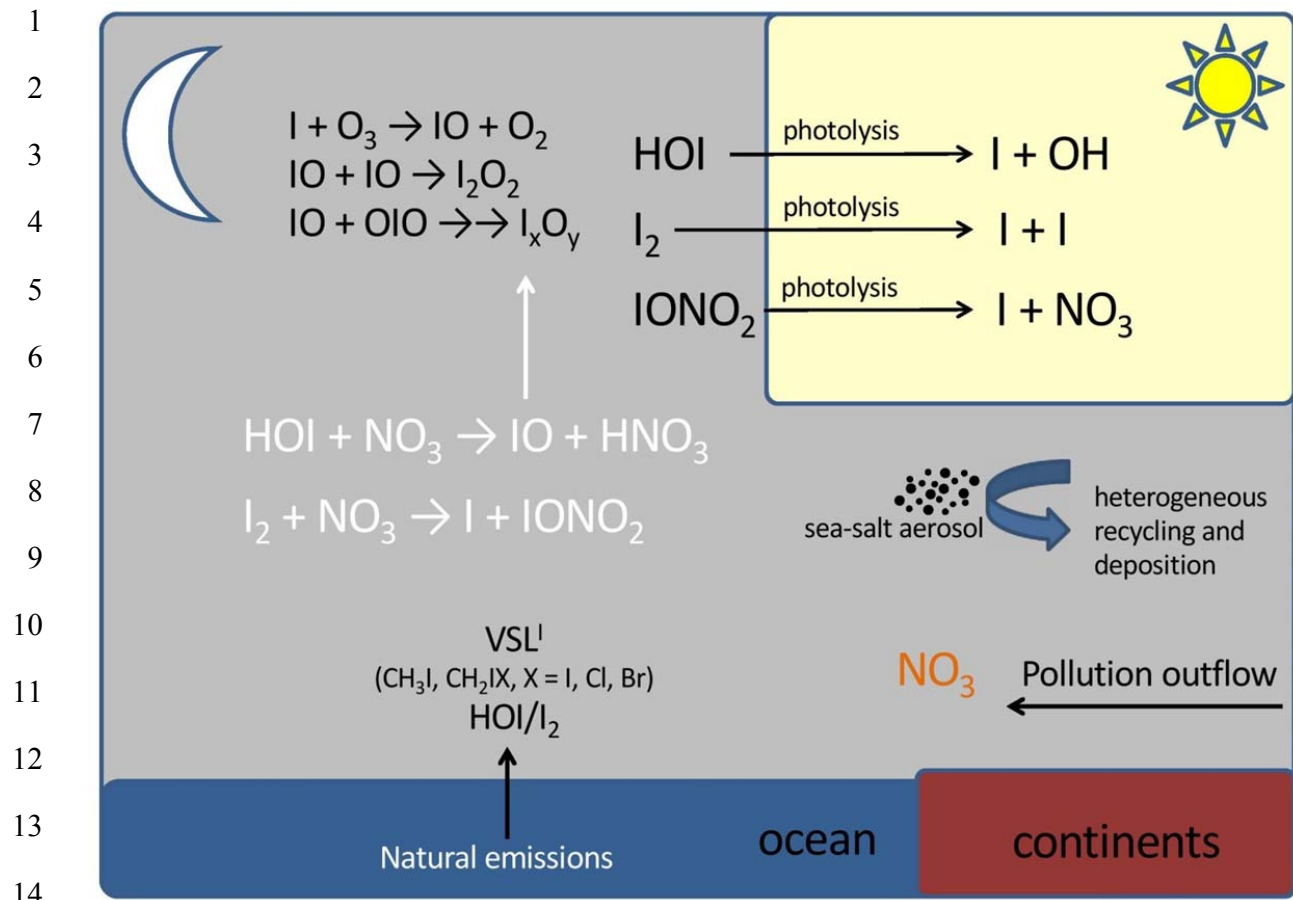
5

6

1 **Table 2.** Calculated vibrational frequencies, rotational constants and energies of the stationary
 2 points and asymptotes on the HOI + NO₃ doublet potential energy surface

Species	Geometry ^a	Vibrational frequencies ^b	Rotational constants ^c	Potential energy ^d
HOI + NO ₃		603, 1084, 3803 & 261, 261, 805, 1108, 1108, 1126	623.9, 8.182, 8.076 & 13.84, 13.84, 6.919	0.0
IOH-NO ₃ complex	O 1.623,0.284,-0.331 H 1.484,-0.657,-0.043 I 0.009,1.205,0.286 N -0.456,-2.265,0.030 O -1.052, -3.321,-0.0473 O -1.147,-1.195,-0.228 O 0.742,-2.161,0.333	55, 84, 118, 161, 196, 615, 629, 667, 705, 803, 968, 1228, 1273,1491, 3268	5.610, 0.916, 0.806	-24.0
IO-H-NO ₂ TS	O 0.309,1.515,0.247 H -0.834,1.314,-0.017 I 1.280,-0.089,-0.093 N -2.349,-0.133,0.019 O -3.518, , -0.429,-0.035 O -1.444,-0.962,0.257 O -2.019,1.117,-0.187	1249i, 70, 97, 103, 225, 472, 676, 698, 797, 806, 1041, 1147, 1308, 1513, 1626	6.300, 0.864, 0.767	-16.4
IO-HNO ₃ complex	O 0.571,1.350,0.348 H -1.111,1.098,-0.020 I 1.870,0.0645,-0.152 N -2.503,-0.202,0.0186 O -3.673,-0.396,-0.170 O -1.654,-0.986,0.401 O -2.081,1.090,-0.242	35, 43, 76, 126, 198, 623, 677, 703, 772, 798, 939, 1331, 1416, 1713, 3281	7.058, 0.605, 0.566	-34.8
IO + HNO ₃		648 & 477, 585, 649, 782, 901, 1320, 1345, 1738, 3724	9.844 & 13.01, 12.05, 6.258	-10.6

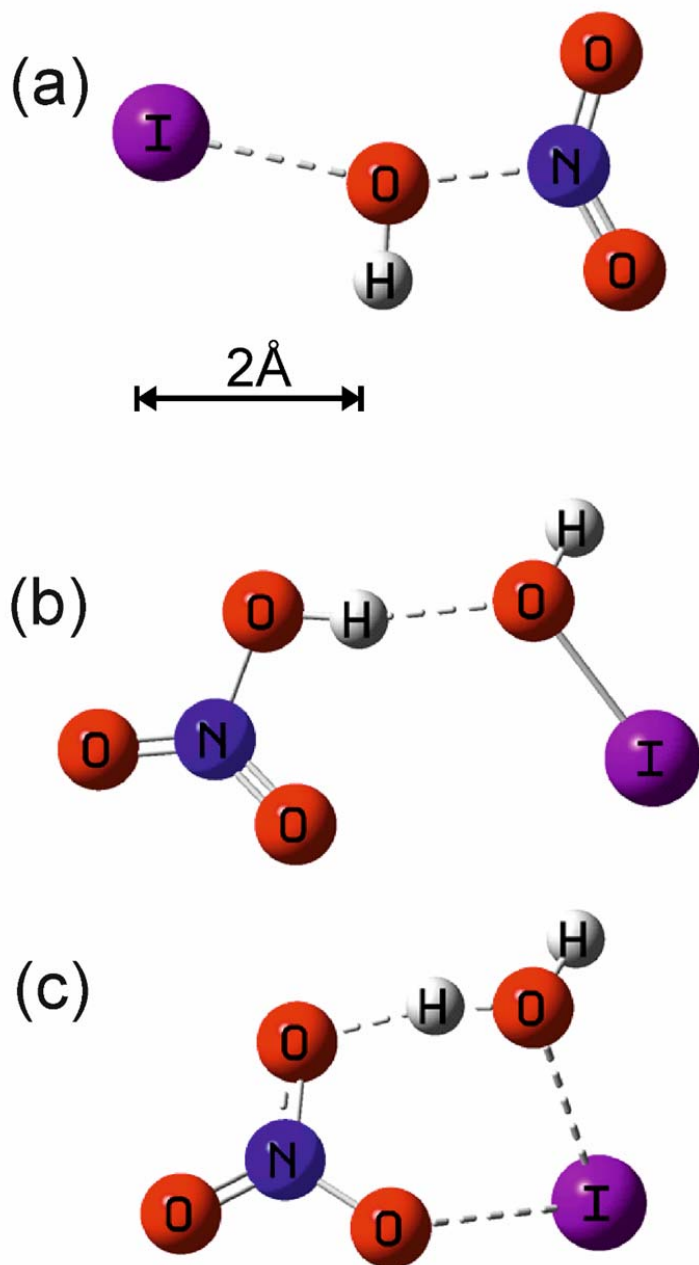
3 ^a Cartesian co-ordinates in Å. ^b In cm⁻¹. ^c In GHz. ^d In kJ mol⁻¹, including zero-point energy and spin-
 4 orbit coupling of I and IO (see text).



15 **Figure 1.** New nocturnal iodine chemistry (in white) implemented in the THAMO and CAM-
 16 Chem models.

17
18
19
20
21
22
23
24
25

1



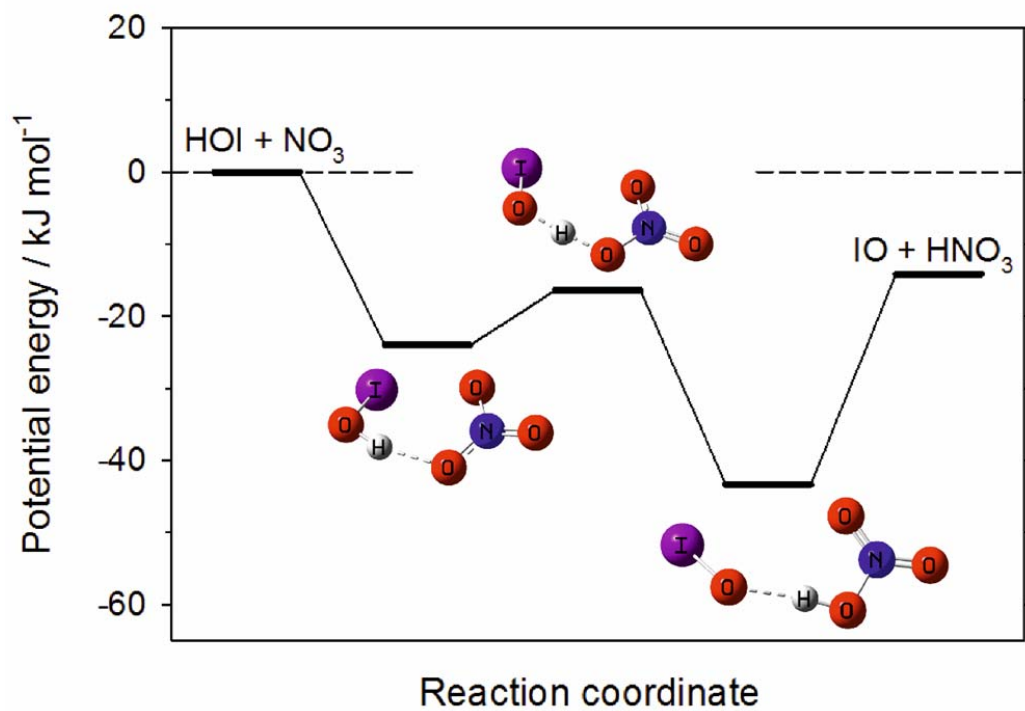
2

3

4

5 **Figure 2:** (a) Transition state for the reaction between HOI and NO₂ to form HNO₃ + I; (b)
6 complex formed between HOI and HNO₃, which then reacts via transition state (c) to form
7 IONO₂ + H₂O.

1

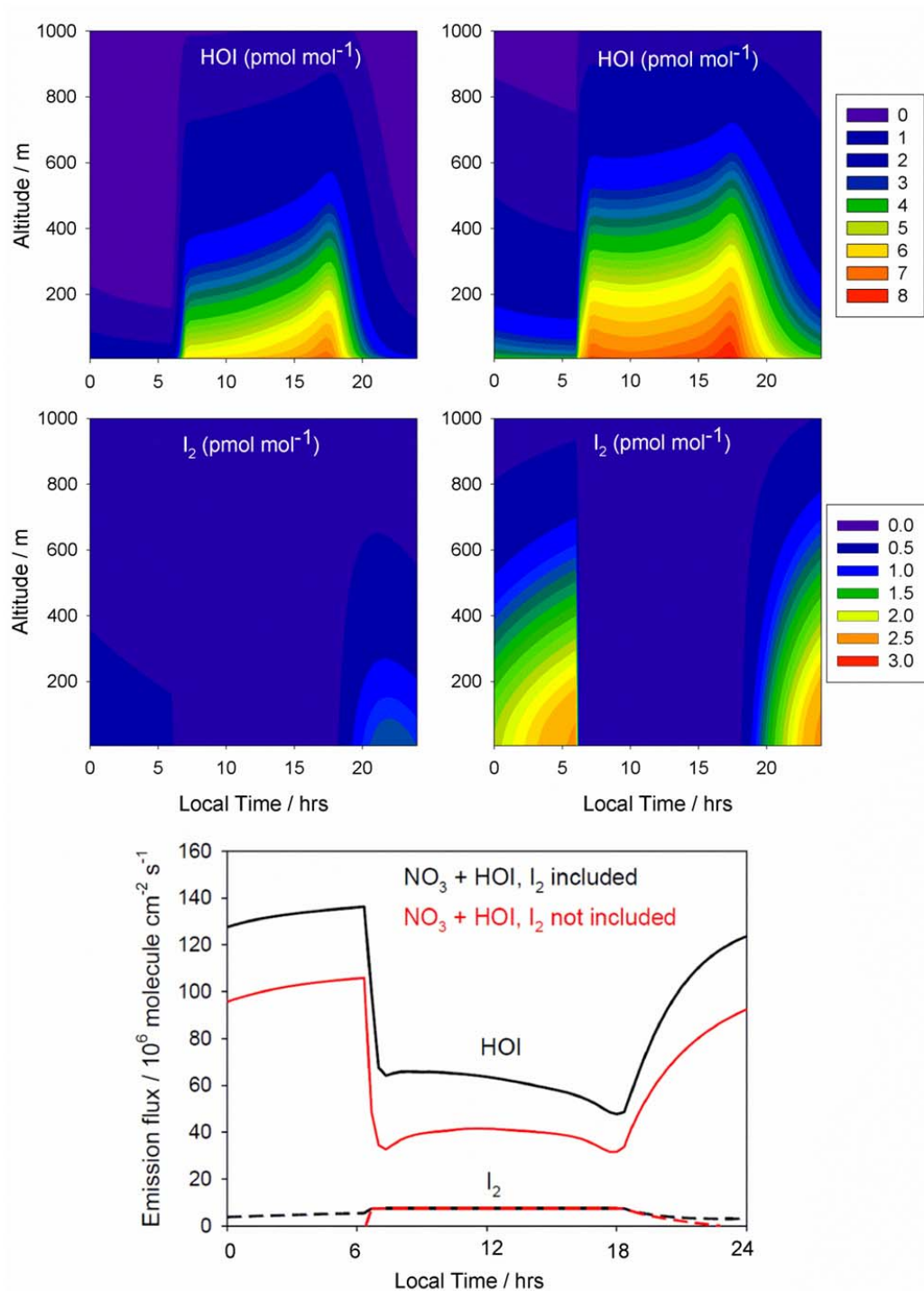


2

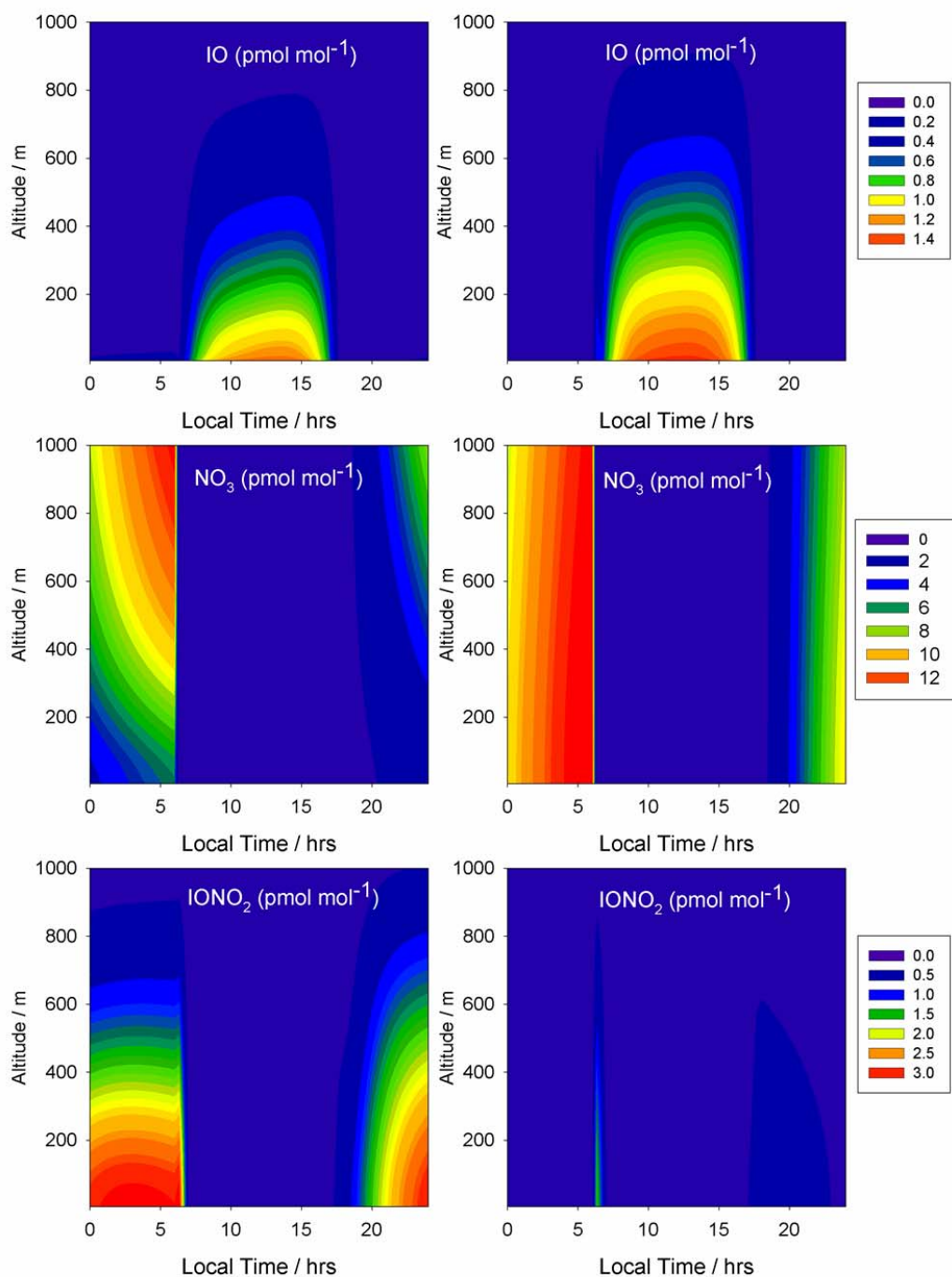
3

4 **Figure 3.** Potential energy surface for the reaction between HOI and NO₃, which contains two
5 intermediate complexes separated by a submerged barrier.

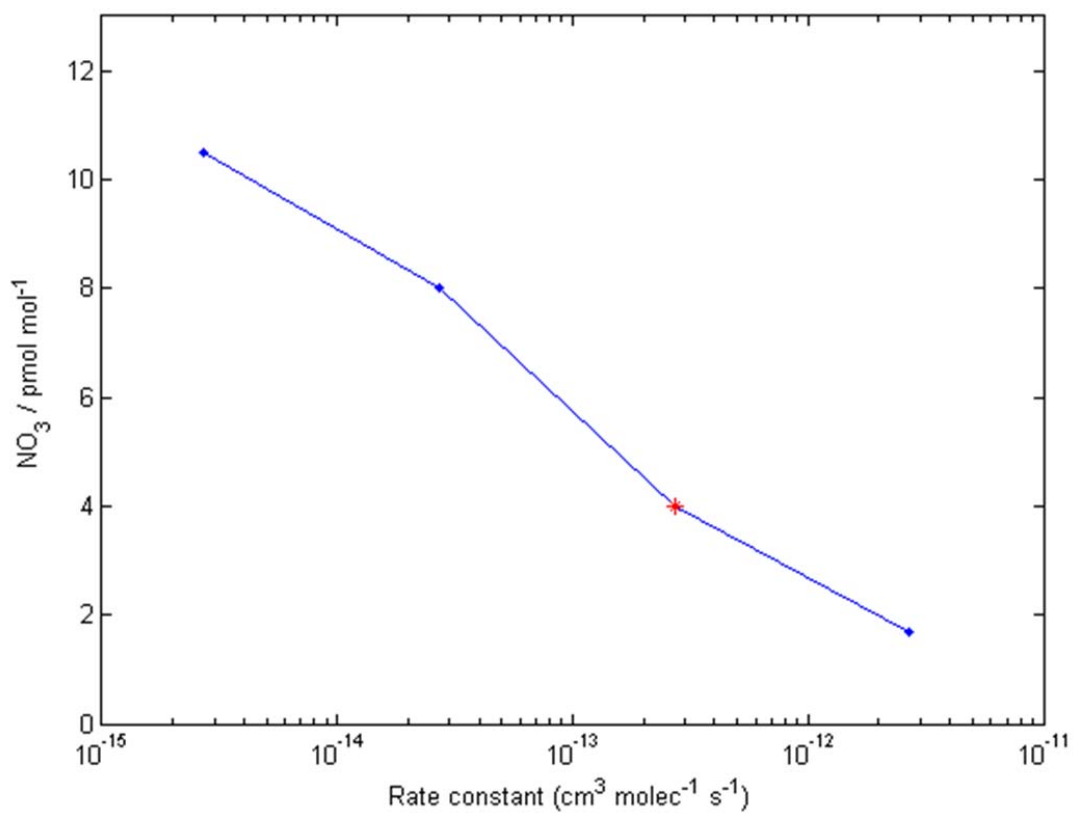
6



1
 2 **Figure 4.** THAMO modeled diurnal variation of HOI, I₂ (upper panels) and the HOI/I₂ flux from
 3 the ocean surface (bottom panel). The right hand panels are from scenario 1, which do not
 4 include night time reactions of HOI and I₂ with NO₃, while the left hand panels include the
 5 reactions in scenario 2. In bottom panel red lines represent scenario 1, while black lines
 6 correspond to scenario 2.



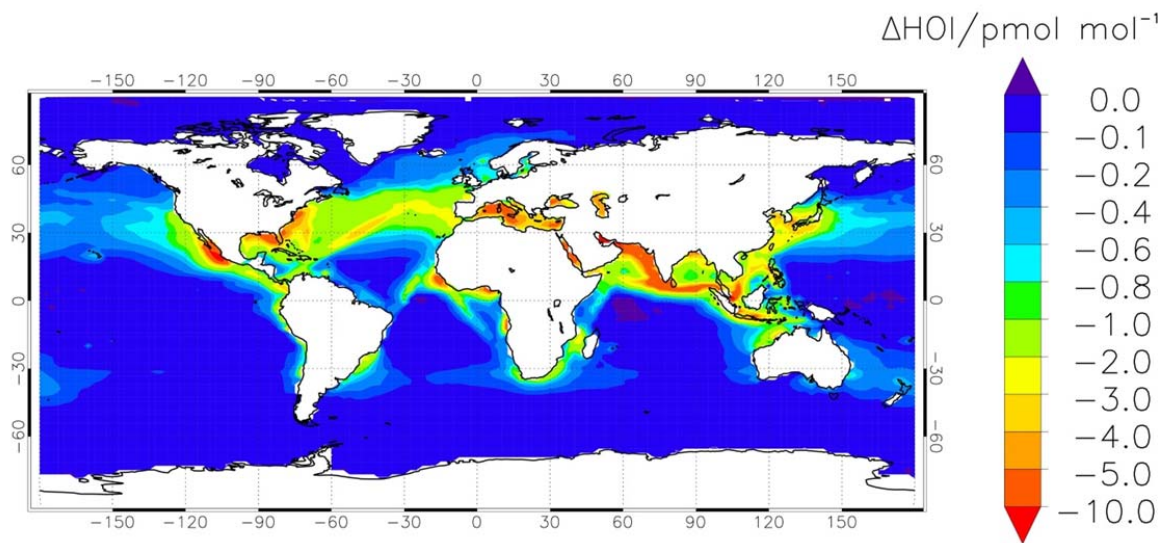
1
 2 **Figure 5.** THAMO modeled diurnal variation of IO, NO₃ and the IONO₂. The right hand panels
 3 are from scenario 1, which do not include night time reactions of HOI and I₂ with NO₃, while the
 4 left hand panels include the reactions in scenario 2.



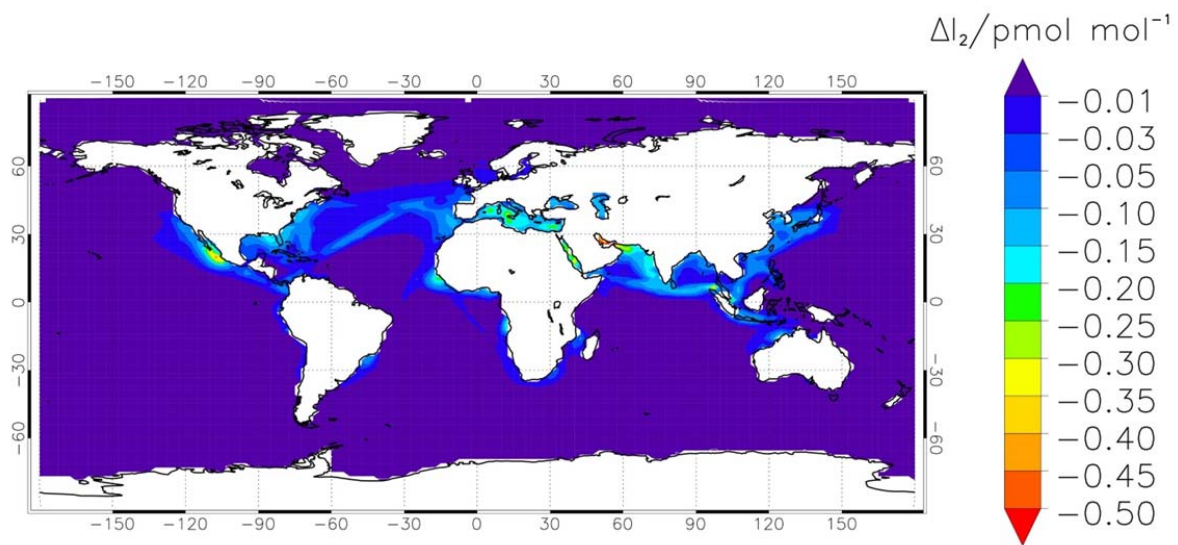
1
2 **Figure 6.** Sensitivity run showing the effect of the uncertainty in the rate constant estimation on
3 the reduction of NO_3 peak nighttime concentration at the surface - the red point is the theoretical
4 estimate.

5
6
7
8
9
10
11

1



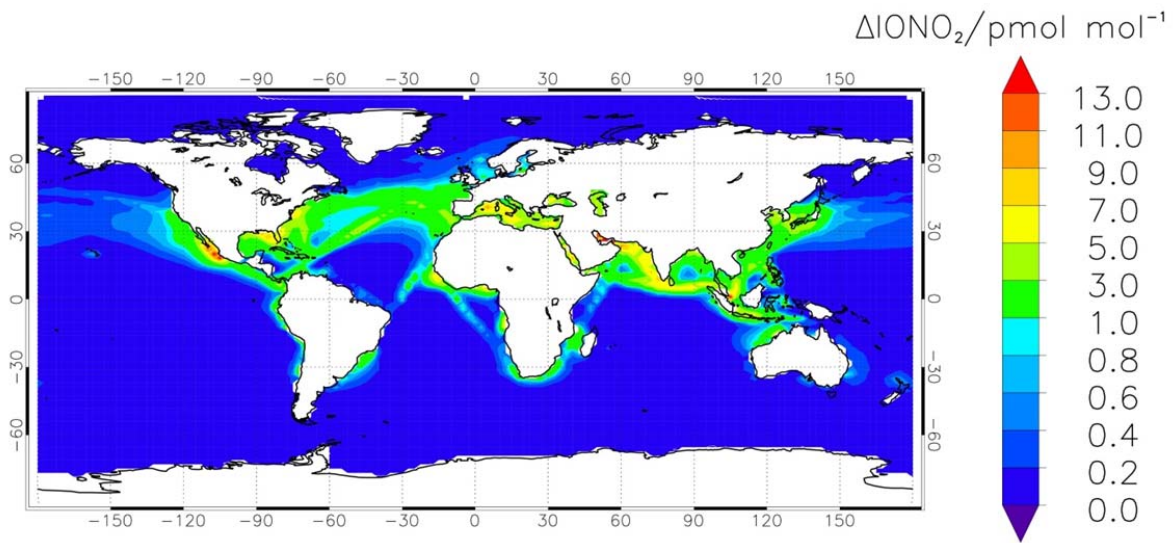
2



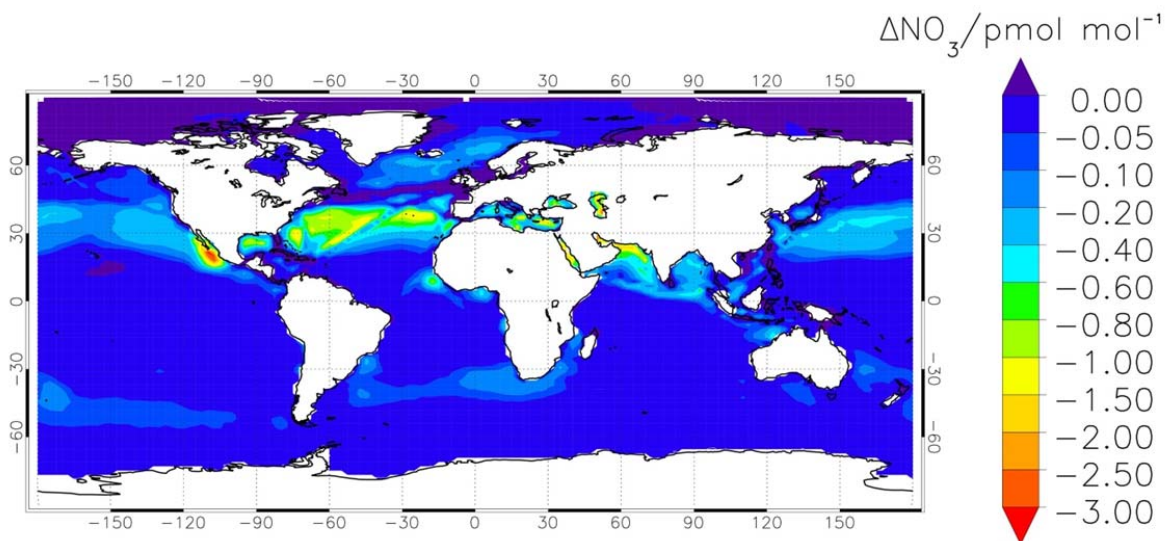
3

4 **Figure 7.** Modelled annual average of HOI (a) and I₂ (b) during night time (from 0:00 to 1:00
5 LT) at the surface level. The panels show the difference in volume mixing ratio between the
6 simulations with and without reactions (1) and (4).

7



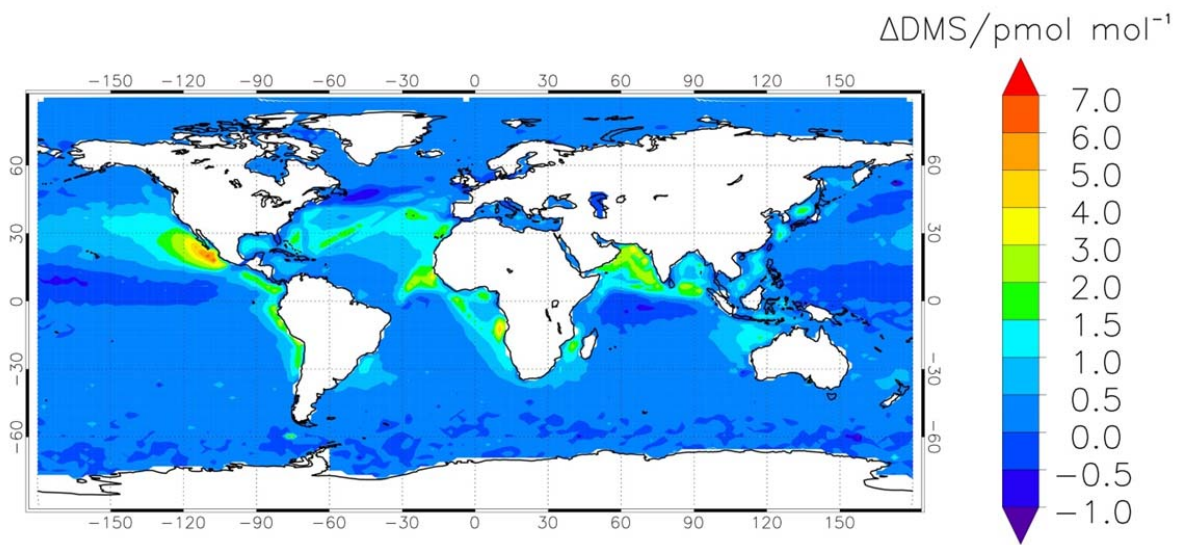
1



2

3 **Figure 8.** Modelled annual average of IONO_2 (a) and NO_3 (b) during night time (from 0:00 to
 4 1:00 LT) at the surface level, as the difference in volume mixing ratio between the simulations
 5 with and without reactions (1) and (4).

6



1

2 **Figure 9.** Increase in the DMS levels during night time (from 0:00 to 1:00 LT) at the surface
 3 level due to the inclusion of the reactions R1 and R4 in CAM-Chem.

4

5

6

7

8

9

10

11

12

13

14

15

16

1
2
3
4
5
6
7
8
9
10
11
12
13
14
15
16
17
18
19
20
21
22
23
24

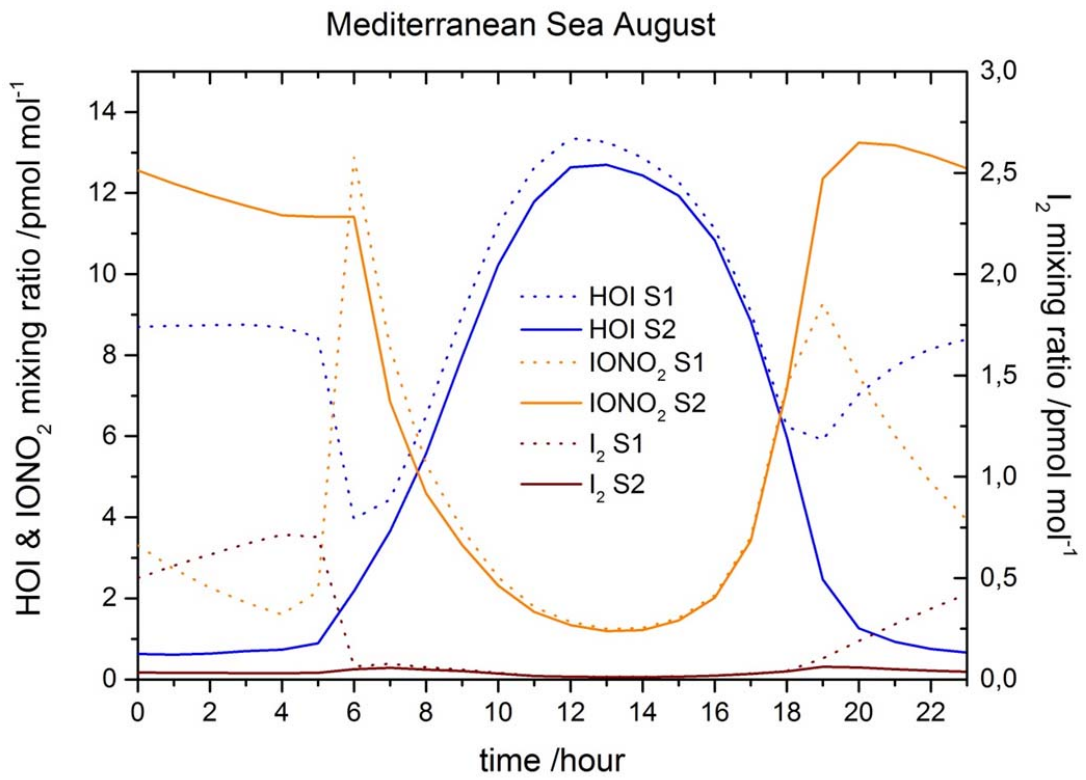
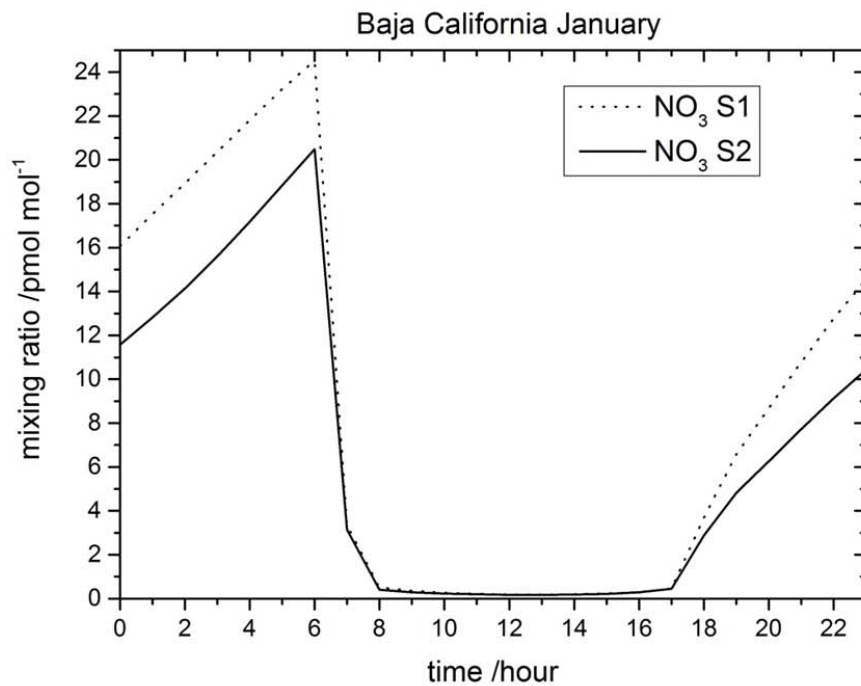
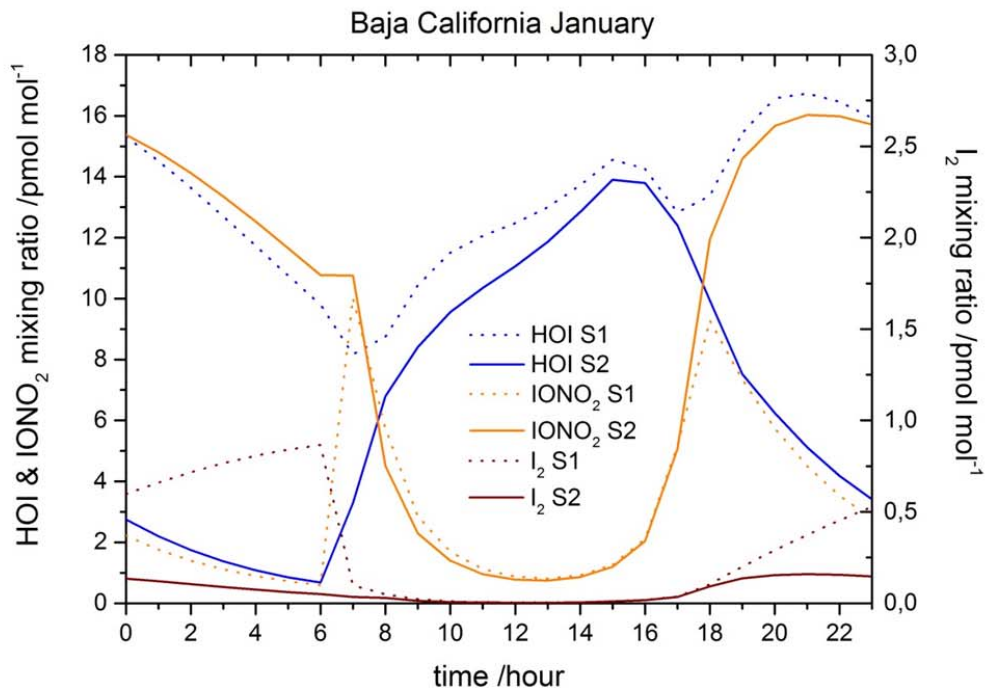


Figure 10. Hourly averaged concentration of HOI, IONO₂ and I₂ in the Mediterranean Sea at the surface level (lon:10°→20°E, lat:33°→40°N)



22 **Figure 11.** Hourly averaged concentration of HOI, IONO₂ and I₂ (upper panel) and NO₃ (bottom
 23 panel) in the Pacific Ocean at the south of Baja California peninsula at the surface level
 24 (lon: -110°→-106°E, lat:16°→23°N)